Experimental Charge Density Studies of Disordered *N*-Phenylpyrrole and *N*-(4-Fluorophenyl)pyrrole

Kathrin Meindl,[†] Julian Henn,[†] Nikolaus Kocher,[†] Dirk Leusser,[†] Klaas A. Zachariasse,[‡] George M. Sheldrick,[†] Tibor Koritsanszky,[§] and Dietmar Stalke*[,†]

Institut für Anorganische Chemie, Georg-August-Universität Göttingen, Tammannstrasse 4, 37077 Göttingen, Germany, Spektroskopie und Photochemische Kinetik, Max-Planck-Institut für Biophysikalische Chemie, Am Fassberg 11, 37077 Göttingen, Germany, and Department of Chemistry, Middle Tennessee State University, MTSU Box 0395, 1301 East Main Street, Murfreesboro, Tennessee 37132

Received: March 23, 2009; Revised Manuscript Received: July 14, 2009

The static electron densities of the title compounds were extracted from high-resolution X-ray diffraction data using the nucleus-centered finite multipole expansion technique. The interpretation of the data collected for the *N*-phenylpyrrole crystal revealed a static disorder that could be successfully resolved within the aspherical-atom formalism. The local and integrated topological properties of the density obtained via a constrained multipole refinement are in statistical agreement with those calculated at the B3LYP/cc-pVTZ level of theory for the isolated molecule and for those derived from the experimental density of the para-fluorinated derivative *N*-(4-fluorophenyl)pyrrole. The topological analysis of the densities indicates neither pyramidal character of the pyrrole N-atom nor a quinoidal structure of the phenyl rings in either molecule. The fluorine substitution appears to have only a minor effect on the density of the remaining constituents but it results in markedly different features of the electrostatic potential of the two compounds. The consistency of the multipole refinement is validated by residual density analysis.

Introduction

In the investigation of intramolecular charge transfer (ICT) in the singlet excited state taking place in electron donor(D)/acceptor(A) molecules, *N*-phenylpyrrole (**PP**) and its derivatives 4-cyano-*N*-phenylpyrrole (**PP4C**) and 4-fluoro-*N*-phenylpyrrole (**PP4F**) have played an important role.[1,2] From the similarity of the ICT reaction of these *N*-phenylpyrroles with their planarized counterparts fluorazene (**FPP**), 4-cyanofluorazene (**FPP4C**), and 4-fluorofluorazene (**FPP4F**), it has been concluded that the ICT state of these molecules has an overall planar structure (Scheme 1).[1] This finding is in support of the planar intramolecular charge transfer model. It, however, contradicts the twisted intramolecular charge transfer approach, which claims that the D and A moieties of a D/A molecule are in a mutual perpendicular configuration in the equilibrated ICT state.[2]

In the discussion of the structural aspects of the ICT reaction with D/A molecules, information on the molecular structure of the electronic ground state (S_0) of these substances is of substantial importance. This structure also plays a role in comparing the results of computations with structural experimental data.[1] In the case of 4-(dimethylamino)benzonitrile and a number of its derivatives, X-ray structure analysis has been an important starting point in the investigation of the structural aspects of the ICT reactions of these molecules.[3] In general, a detailed analysis of the bonding situation of the N-atom at the electronic level of molecules such as **PP** and **PP4F** in the electronic ground state S_0 is thus important for a better understanding of the structural changes accompanying and governing excited state processes in such A/D molecules.

The solid state electron density can be derived by an X-ray diffraction experiment, provided accurate high-resolution Bragg intensity data are interpreted within an aspherical-atom formalism such as the nucleus-centered multipole expansion model.[4] Since the success of this procedure is subject to the applicability of the kinematical theory of diffraction, experimental charge density studies have consistently avoided systems for which noncoherent, inelastic scattering cannot be neglected or corrected for. In many of these systems the translation symmetry is temporarily destroyed by local structural changes due to electronic or thermal transitions. Recent advances in data collection have opened new perspectives to study dynamic processes. It is now feasible to collect several data sets within a short period of time, extending the data analysis by a new dimension, such as temperature[5] or time.[6] A static structure disorder, i.e., a disorder that persists at any temperature, can—in contrast to dynamic disorder—in principle be resolved from accurate high-resolution data using the conventional structure factor model. Currently, most charge density studies start from entirely ordered small molecule structures.[7] Adequate modeling of disordered sites, however, becomes essential as X-ray density determination is being extended to large systems.[8]

In this paper we describe a constrained multipole refinement protocol that led to a reliable static electron density of the disordered **PP** molecules. The success and reliability of disorder modeling was proven by a residual density analysis.[9] In this approach, a measure of total deviations of the model from the data in a volume under consideration is given by e_{gross}, the gross residual electrons. Therefore, a lower value of e_{gross} indicates a progress in modeling. Furthermore, the whole residual density distribution of the entire unit cell is mapped onto a two-dimensional graph. This graph, the fractal dimensionality distribution of the residual density, reveals even tiny disorder or any other structural information present in the residual density

* To whom correspondence should be addressed. E-mail: dstalke@chemie.uni-goettingen.de.
[†] Georg-August-Universität Göttingen.
[‡] Max-Planck-Institut für Biophysikalische Chemie.
[§] Middle Tennessee State University.

10.1021/jp9026157 CCC: $40.75
Published on Web 08/12/2009

SCHEME 1: Molecular Structures of PP, PP4F, FPP, and FPP4F

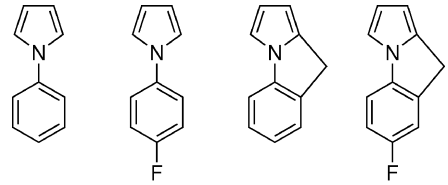

by deviations from the ideal parabolic shape. The results for **PP** are furthermore compared to those obtained experimentally for the para-fluorinated derivative **PP4F** (Figure 1) and to those derived by quantum chemical calculations at the B3LYP/cc-pVTZ level of theory for the corresponding isolated molecules.

Experimental Methods

Data Collection and Processing. The data for both compounds were collected on a Bruker Apex-CCD diffractometer with a D8 three-circle goniometer using graphite-monochromated Mo Kα radiation ($\lambda = 0.71073$ Å) and the SMART control software.[10] The oil-coated crystals were mounted on the tip of a glass fiber. To minimize thermal motion, the measurement was performed at 100(2) K, employing an open circle liquid nitrogen cooling device.[11] The data were collected in ω-scan mode with variable φ-positions at a sample-to-detector distance of 5 cm. The data for the "low-angle batch" were measured at a detector position of $2\theta = 32°$ with a step width of 0.2° per frame, while for the "high-angle batch" the detector position was set to $2\theta = 75°$ with a step width of 0.2° per frame. This strategy resulted in a completeness of 99.6% and 99.9% for **PP** and **PP4F** for the resolution of $(\sin\theta/\lambda)_{max} = 1.05$ Å^{-1} and $(\sin\theta/\lambda)_{max} = 1.00$ Å^{-1}, respectively. To avoid scaling problems due to the limited number of reflections present in both batches, all reflections of the high-angle batch that were also present in the low-angle batch were removed and the two batches were processed independently. In all subsequent refinements, individual scale factors were assigned to the two batches. More details of the data collections are presented in Table 1.

The reflections were integrated with the program SAINT[12] using orientation matrices determined with SMART. Reflections above $\sin\theta/\lambda = 1.05$ Å^{-1} for **PP** and 1.00 Å^{-1} for **PP4F** were excluded from the refinements (Table 2). The raw data were scaled using SADABS[13] and the space group determinations and merging were performed with XPREP.[14]

Structure Refinements. Both structures were solved with the program SHELXS[15,16] using direct methods. The conventional refinements based on the independent-atom model (IAM) were carried out with SHELXL.[17,16] The coordinates and anisotropic displacement parameters (ADP) of the non-hydrogen atoms were initially refined against high-order reflections ($\sin\theta/\lambda \geq 0.80$ Å^{-1}) since the bias introduced by the IAM is negligible beyond this limit.[18] The hydrogen atoms were placed at calculated positions with constrained C—H distances of 0.95 Å and refined using a riding model. The U_{iso}(H) values were set to $1.2U_{eq}$(C) of the carbon atoms they are attached to. After convergence had been reached, the hydrogen atom positions were shifted along the bond vectors to distances in accord with neutron diffraction data.[19]

The detailed inspection of the low-order reflections (in terms of figures of merit such as the internal agreement factor for the symmetry equivalents R_{int} or the R_σ value) and the parameter estimates obtained after initial refinements of **PP** led to promising results with excellent intensity statistics and residual density peaks exclusively located in the bonds. Hence, the data collection was completed up to a resolution of $(\sin\theta/\lambda)_{max} = 1.069$ Å^{-1}. However, the residual density based on all data showed features characteristic of disordered structures; the peaks were no longer located in the bonds but close to atomic positions (Figure 2a,b).

The residual density peaks were identified as the non-hydrogen atoms of the minor component. The occupancies of the two components, which are related by a twofold rotation about an axis normal to the molecular plane through the C—N bond, refined to 90% and 10%, respectively. Distance and similarity restraints were applied. The ADPs of the atoms of the minor component were constrained to match those of the major component. After convergence of the high-order refinement, the hydrogen positions were shifted to neutron positions, leading to the starting model for the multipole refinement.[19]

Multipole Refinements. Multipole refinements using the Hansen-Coppens formalism[4] implemented in the XD program package[20] were carried out against F^2 with reflections $F^2 > 2\sigma(F^2)$ and statistical weights of $1/\sigma^2(F^2)$. Default radial functions were chosen for the core, spherical valence, and deformation densities.[21] The multipole expansion was terminated at the dipolar ($l = 1$) and octapolar ($l = 3$) level for the hydrogen and non-hydrogen atoms, respectively, while the F-atom in **PP4F** was described at the hexadecapolar level ($l = 4$). Atoms at general positions were constrained to obey local mirror plane symmetry, the plane being defined by bond vectors to adjacent non-hydrogen atoms. Hydrogen atoms were grouped according to the chemical similarity of the C-atoms. The shifts in the monopole populations were subject to an electroneutrality constraint in each refinement cycle. A detailed description for the individual structures follows in the next two paragraphs.

Multipole Model for the Disordered Structure of PP. The structure was first refined with XD without taking the disorder into account. Figure 3a shows the corresponding residual density of the multipole refinement. The residual density distribution of the entire unit cell is far from being parabolic in shape (Figure 3b), which proves the existence of non-Gaussian (i.e., systematically) distributed residual density. The residual density distribution is not symmetric as the positive shoulder is much wider and more structured in comparison to the negative one. A positive residual density value stems from regions where the "observed" density is higher than the model density; therefore, a neglected disorder typically generates a large positive residual density shoulder. The flatness, i.e., the difference between the maximum and the minimum residual density value, is, in view of the light atoms, with 0.89 e Å^{-3} high as is the total integrated absolute residual density value of $e_{gross} = 15.93$ e. The flatness appears as width of the baseline in the residual density plot.

For taking the disorder into account, the refinement was constrained in terms of linear equations involving different variables in XD. The ADPs of the non-hydrogen atoms of the minor component were restricted according to a segmented rigid-body model treating the phenyl and pyrrole rings as two independent rigid groups and thus allowing only for relative librational and translational displacements about the C11—N2 bond. This was achieved by starting from averaged U_{iso} values for the non-hydrogen atoms and invoking a necessary number of rigid-link constraints on the shift of ADPs. Carbon atoms exhibiting the same connectivity in each ring were considered chemically equivalent. This corresponds to imposing a pseudo mirror plane normal to the plane of each ring through the C—N bond vector. The deformation density of the minor component

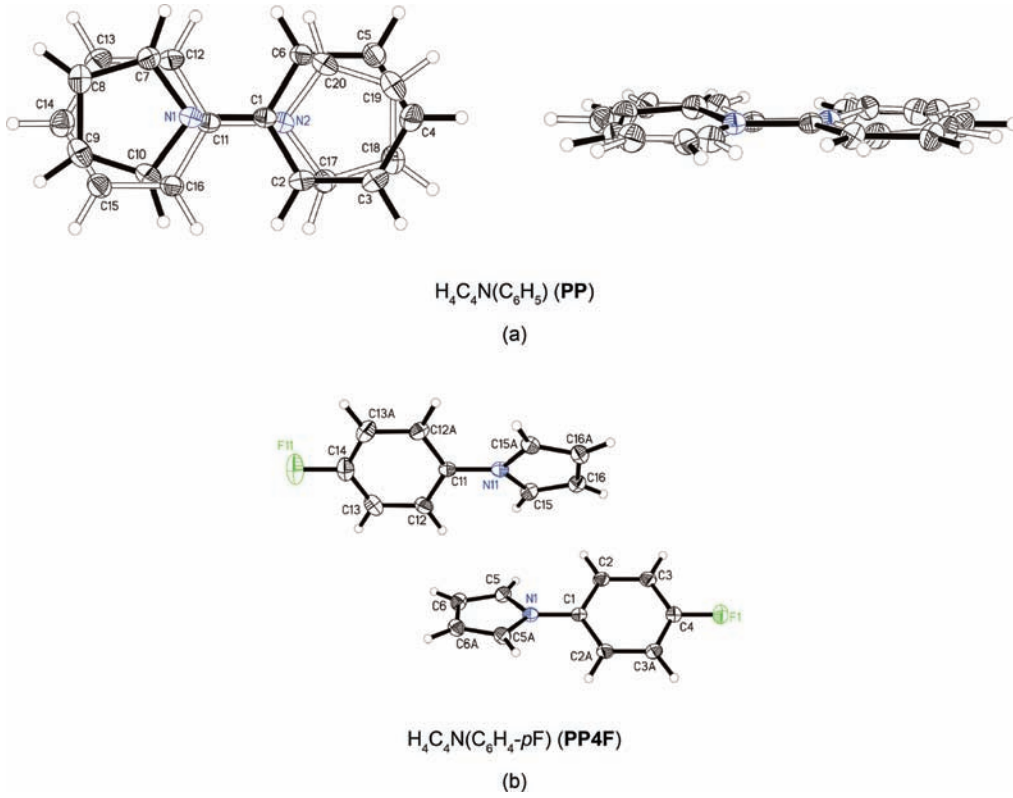

Figure 1. Molecular structures of **PP** (a) (left, top view; right, side view) and **PP4F** (b). Anisotropic displacement parameters are depicted at the 50% probability level. The major component of **PP** is drawn in black and the minor component in white.

TABLE 1: Details of the Data Collection of Compounds PP and PP4F

	PP	**PP4F**
crystal size [mm^3]	0.40 × 0.20 × 0.05	0.40 × 0.40 × 0.05
temperature [K]	100	100
detector positions (2θ) [deg] (low angle, high angle)	32, 75	32, 75
φ-positions (low angle) [deg]	0, 45, 90, 135, 180, 225, 270, 315	0, 90, 180 (2 times each), 45, 135, 225, 270, 315
no. of frames per run/$\Delta\omega$ [deg]/exposure time [s]	895/−0.2/10	895/−0.2/10
φ-positions (high angle) [deg]	0, 45, 90, 180, 225, 270	0, 45, 90, 135, 180, 225, 270, 315
no. of frames per run/$\Delta\omega$ [deg]/exposure time [s]	895/−0.2/90	901/−0.2/60
$(\sin\theta/\lambda)_{max}$ [Å^{-1}]	1.069	1.041
reflections collected (low-angle batch)	20609	29212
reflections collected (high-angle batch)	25467	45273

was demanded to be the same as that of the major component (P_{lm}(C3) = P_{lm}(C5) = P_{lm}(C13) = P_{lm}(C15), P_{lm}(C2) = P_{lm}(C6) = P_{lm}(C12) = P_{lm}(C16) in the phenyl rings and P_{lm}(C7) = P_{lm}(C10) = P_{lm}(C17) = P_{lm}(C20), P_{lm}(C8) = P_{lm}(C9) = P_{lm}(C18) = P_{lm}(C19) in the pyrrole rings). Individual radial expansion/contraction parameters κ were assigned to each chemically unique atom, leading to six κ-sets. However, the deformation screening parameters (κ') for the C- and H-atoms were fixed to values obtained from model refinements against theoretical structure factors.[22]

Figure 4a shows the residual density after a multipole refinement, taking the disorder into account. The residual density map is featureless after the multipole refinement accounting for the disorder (Figure 4b).

The number of gross residual electrons, which describes all model inadequacies and noise in the data, falls to 6.16 e and the flatness of the residual density decreases to 0.23 e Å^{-3}. For a comparison of residual density descriptors prior to and after taking disorder into account, see Table 3. All ADPs of the major component are consistent with the rigid-bond criterion of Hirshfeld,[23] indicating a proper deconvolution of the electron density from thermal motion. Please note that only the minor component was subject to rigid-link constraints.

Multipole Model for PP4F. The asymmetric unit of **PP4F** contains two half molecules. To stabilize the preliminary refinement and to reduce the number of parameters, the multipole coefficients of the corresponding atoms in the two molecules were constrained to be the same. The complexity of the model was increased in a stepwise manner, starting with the adjustment of the scale factors, followed by adjustment of the monopole populations (P_v) together with the radial screening parameters (κ), followed by the multipole populations (P_{lm}) of the non-hydrogen atoms. Positional parameters and ADPs of the non-hydrogen atoms were refined thereafter. The parameters of the hydrogen atoms were kept fixed at the values of the starting model until the coordinates and ADPs of the non-hydrogen atoms were included in the refinement. They were adjusted after each step of the refinement using only the reflections with $\sin\theta/\lambda \leq 0.5$ Å^{-1}, keeping the C—H distances fixed and restraining the U_{iso}(H) values. P_v and P_{lm} of all atoms were refined together with positional and thermal motion parameters of the non-hydrogen atoms and with the scale factors.

TABLE 2: Crystallographic Data for Compounds PP and PP4F

	PP	PP4F
crystal system	orthorhombic	monoclinic
space group	$P2_12_12_1$	$P2/c$
a [Å]	5.6405(2)	9.2746(2)
b [Å]	7.5996(2)	10.8053(3)
c [Å]	17.6532(2)	9.0264(2)
β [deg]	90	118.810(2)
V [Å^3], Z	756.60(13), 4	792.61(3), 4
μ [mm^{-1}]	0.07	0.10
reflections used in the multipole refinement[a]	3746	5465
$(\sin\theta/\lambda)_{max}$ [Å^{-1}][a]	1.05	1.00
completeness to $(\sin\theta/\lambda)_{max}$ [%][a]	99.6	99.9
no. of unique reflections (low-angle batch)/R_{int}[a]	910/0.0060	1575/0.0270
no. of unique reflections (high-angle batch)/R_{int}[a]	2836/0.0234	3890/0.0687
limiting indices	$-12 \le h \le 12$	$-18 \le h \le 16$
	$0 \le k \le 16$	$0 \le k \le 22$
	$0 \le l \le 38$	$0 \le l \le 18$
R1 ($I > 2\sigma(I)$) after IAM refinement to $(\sin\theta/\lambda)_{max}$[a]	0.0399	0.0527
wR2 ($I > 2\sigma(I)$) after IAM refinement to $(\sin\theta/\lambda)_{max}$[a]	0.1079	0.1428
R1 ($I > 2\sigma(I)$) after multipole refinement to $(\sin\theta/\lambda)_{max}$[a]	0.0268	0.0581
wR2 ($I > 2\sigma(I)$) after multipole refinement to $(\sin\theta/\lambda)_{max}$[a]	0.0332	0.0518
GoF	2.61	2.50
N_{refl}/N_{param}	17.03	29.70

[a] The cutoffs $(\sin\theta/\lambda)_{max}$ and $I > 2\sigma(I)$ were applied.

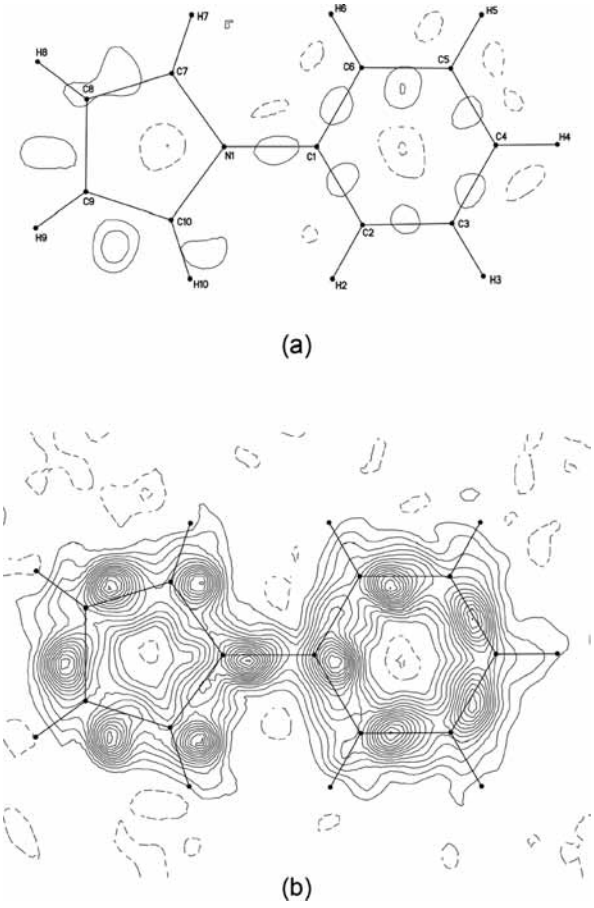

Figure 2. Contour plots of the residual densities of **PP** after IAM refinement without taking the disorder into account: (a) refinement with reflections up to $(\sin\theta/\lambda)_{max} = 0.625$ Å^{-1}; (b) refinement with reflections up to $(\sin\theta/\lambda)_{max} = 1.05$ Å^{-1} and atomic positions from a high-order refinement with $(\sin\theta/\lambda)_{min} = 0.85$ Å^{-1}. Contour step width is 0.1 e Å^{-3}; positive contours are drawn in solid and negative contours in dashed lines.

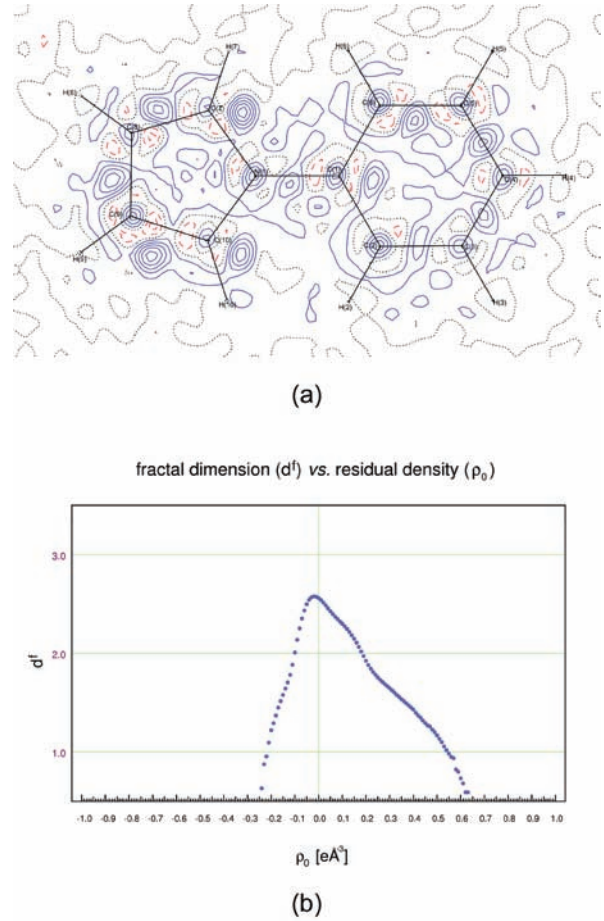

Figure 3. (a) Contour plot of the residual density after multipole refinement of **PP** without taking the disorder into account; positive contours are drawn in solid lines, negative contours are drawn in dashed lines, and the zero contour line is dotted, the step width being 0.1 e Å^{-3}. (b) Fractal dimensionality distribution of the residual density in the whole unit cell. The residual density flatness $\Delta\rho_0$ is 0.89 e Å^{-3}.

Subsequently, three sets of expansion/contraction parameters of the deformation radial functions (κ') were introduced for the chemically distinct C-atoms. For the hydrogen atoms, κ and κ' values suggested by Volkov et al. were used and kept fixed

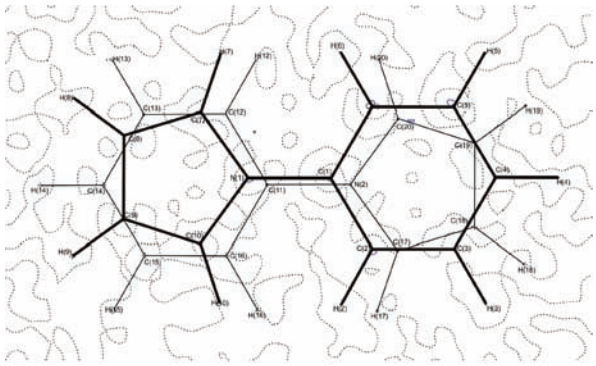

(a)

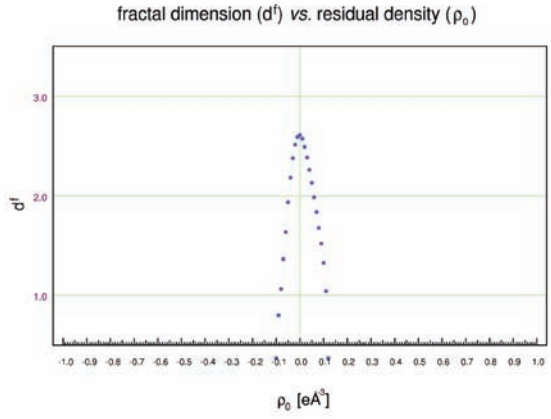

(b)

Figure 4. (a) Contour plot of the residual density after multipole refinement of **PP** with disorder taken into account; the major disorder component is shown with bold lines. Positive contours are drawn in solid lines, negative contours are drawn in dashed lines, and the zero contour line is dotted, the step width being 0.1 e Å^{-3}. (b) Fractal dimensionality distribution of the residual density in the whole unit cell after the inclusion of disorder. The residual density flatness $\Delta\rho_0$ is 0.23 e Å^{-3}.

TABLE 3: Residual Density Descriptors Calculated on a 56 × 76 × 176 Grid prior to and after Taking Disorder into Account within the Multipole Model

	$d^f(0)$[a]	e_{gross}[b] [e]	$\Delta\rho_0$[c] [e Å^{-3}]
disordered **PP**	2.5589	15.93	0.89
disorder modeled **PP**	2.6120	6.16	0.23

[a] $d^f(0)$ indicates the value of the fractal dimensionality for the residual density value zero. This value is dependent solely on the residual density grid size, the experimental resolution, and the density model. In most cases a greater value indicates decreasing features in the residual density. [b] e_{gross} describes the total amount of density badly accounted for; it may stem from model inadequacies or from noise in the data. In the latter case the fractal dimensionality distribution of the residual density is parabolic in shape. [c] $\Delta\rho_0$ indicates the flatness of the residual density distribution (highest residual density peak minus lowest residual density hole). The density model fitting procedure minimizes the flatness.

during the refinement of both compounds.[22] In the final step, all parameters except for κ' of all non-hydrogen atoms and x, y, z, and U_{iso} of the hydrogen atoms were refined together.

Results and Discussion

All numbers given for **PP** refer to the major domain if not stated otherwise. In **PP** and its para-fluorinated derivative **PP4F** the nitrogen atom is part of a five-membered ring. A comparison of the geometrical features around this N-atom with those of aminobenzonitriles with a noncyclic group is of considerable interest. The twist angle, defined as the angle between the plane of the pyrrole and the phenyl ring, is only 5.8° for **PP** and increases to 22.3° and 27.9° in the two **PP4F** molecules in the asymmetric unit. From theoretical calculations (B3LYP/cc-pVTZ[24]) dihedral angles of 35.2° for **PP** and 37.6° for **PP4F** are obtained. The sum of the angles around the nitrogen atom indicates the absence of a pyramidal character caused by a stereochemically active lone pair. In both compounds this sum is close to 360°, the ideal value for a planar N(sp^2) atom, but considerably different from that often found for 4-(dialkylamino)-benzonitriles.[3,25]

In contrast to the observations regarding some 4-aminobenzonitriles,[3] there is no indication for a quinoidal structure of the phenyl ring in either molecule. Such a partial quinoidal character would be evident from different bond lengths in the phenyl ring (i.e., the C2—C3/C5—C6 bond in **PP** and the C2—C3 and the C12—C13 bonds in **PP4F** would be shorter). The differences in the C—C bond lengths, however, only scatter around 0.01 Å. The N-phenyl bond lengths (1.4201(7) Å in **PP**; 1.4153(13) Å (N1—C1) and 1.4197(13) Å (N11—C11) in **PP4F**) are slightly longer than the standard N(sp^2)—C(sp^2) single bond.[26] This suggests a relatively free rotation about the N-phenyl bond. Inversion at the N(sp^2) atom in the pyrrole ring can be excluded.

A head-to-tail herringbone stacking of the molecules is found in the crystal of **PP**, with molecules clearly deviating from a coplanar arrangement. In the crystal of **PP4F** the molecules form chains via bifurcated (C—H)$_2$···F—C hydrogen bonds. Every second chain points in the opposite direction. The angle between the two mean planes of the chains is almost exactly rectangular (90.3°). The distance between fluorine and the hydrogen atoms of neighboring molecules is 2.725 Å for one set of independent molecules and 2.720 Å for the other. Both distances are in the range quoted for weak C—H···F—C hydrogen bonds (Figure 5).[27]

Electron Density and Related Electronic Properties. Local and integrated topological properties of the experimental density were evaluated with XDPROP,[20] while the theoretical properties (B3LYP/cc-pVTZ[24]) were calculated with AIM2000[28] and DGrid.[29] These include the BCP locations, the density $\rho(\mathbf{r}_{BCP})$, and the Laplacian $\nabla^2\rho(\mathbf{r}_{BCP})$ at these sites and along the bond paths, and the AIM charges and volumes from the integration over the atomic basins.[30] The experimentally and theoretically derived bond properties of the most important bonds are given in Table 4.

The BCP properties (ρ_{BCP} and $\nabla^2\rho_{BCP}$), providing also sensitive measures of the covalent/ionic character of a bond, can moreover be used for quantitative validation of model densities. Instead of direct comparison of these topological figures for each chemically equivalent bond in different molecules, derived either from theoretical or experimental densities, we use here the mean of their absolute deviations (MAD)—calculated with the inclusion of all bond pairs to be compared—as overall reliability indices. The comparative topological analysis of the theoretical densities of **PP** and **PP4F** allows for estimation of the effect of fluorine substitution on the bonds. The MAD values based on six bond pairs (due to the mirror symmetry, only two C—N and four C—C bonds, excluding the (F)C—C bond, are considered) are found to be 0.002 e Å^{-3} and 0.096 e Å^{-5} for ρ_{BCP} and $\nabla^2\rho_{BCP}$, respectively. This indicates a negligible substitution effect; that is, the bonds

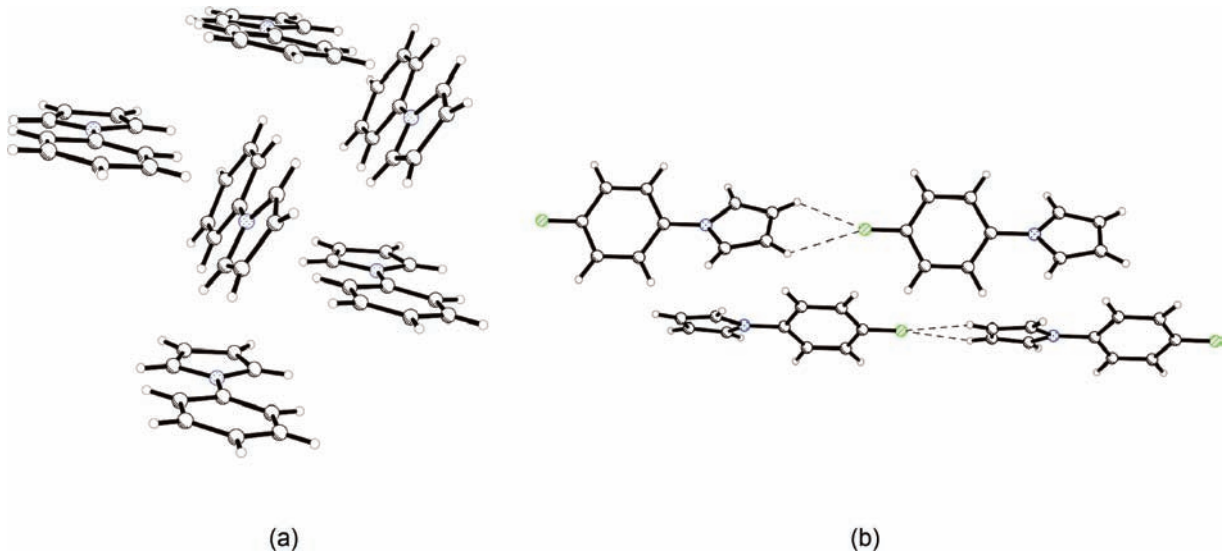

Figure 5. Crystal packing in (a) $H_4C_4N(C_6H_5)$ (**PP**) and (b) $H_4C_4N(C_6H_4$-*p*F) (**PP4F**).

TABLE 4: Experimentally and Theoretically Derived Topological Properties of the C_{ipso}—N and C—F Bonds in PP and PP4F at the BCP[a]

compound	A—B	*d*(A—B)[b] [Å]	*d*(A—BCP) [Å]	*d*(BCP—B) [Å]	$\rho(\mathbf{r}_{BCP})$ [e Å^{-3}]	$\nabla^2\rho(\mathbf{r}_{BCP})$ [e Å^{-5}]
PP	C1—N1	1.4201(7)	0.5850	0.8352	1.935(5)	−15.397(45)
		1.4143	*0.5355*	*0.8788*	*1.9578*	*−20.5674*
PP4F	C1—N1	1.4153(13)	0.5852	0.8301	2.063(8)	−18.575(33)
		1.4146	*0.5374*	*0.8772*	*1.9588*	*−20.5997*
PP4F	C11—N11	1.4197(13)	0.5714	0.8483	2.024(12)	−17.709(49)
PP4F	C4—F1	1.3561(16)	0.5718	0.7842	2.066(15)	−14.862(57)
		1.3490	*0.4469*	*0.9021*	*1.7783*	*0.3207*
PP4F	C14—F11	1.360(2)	0.5318	0.8279	1.975(20)	−18.172(86)

[a] Values in italics are from the theoretical calculations of **PP** and **PP4F**.[28] [b] *d*(A—B) is the bond length between the atoms A and B, *d*(A—BCP) and *d*(BCP—B) denote the distances of the atoms A and B from the BCP, respectively, $\rho(\mathbf{r}_{BCP})$ is the charge density, and $\nabla^2\rho(\mathbf{r}_{BCP})$ is the Laplacian at the BCP.

in **PP4F**, excluding those to the fluorinated C-atom, are indeed equivalent with the corresponding bonds in **PP**. The comparison of the experimental densities of the two symmetry independent **PP4F** molecules in terms of five C—C and two C—N bond pairs leads to MAD values of 0.065 e Å^{-3} and 1.435 e Å^{-5}. The comparison of the experimental BCP properties of **PP** with those of the same bonds (averaged over the two molecules) in **PP4F** gives MAD values of 0.074 e Å^{-3} and 2.416 e Å^{-5}. The theory versus experiment analysis, however, results in 0.068 e Å^{-3} and 6.625 e Å^{-5} for the MADs in **PP** and 0.050 e Å^{-3} and 4.662 e Å^{-5} in **PP4F**. This simple test suggests an internal consistency for the experimental densities and it validates the reliability of the density of the disordered **PP** molecule. In other words, the uncertainty in the BCP properties derived for the two compounds from independent data is comparable with the uncertainty in reproducing these properties for the two chemically identical **PP4F** molecules from the same data. The results are also in line with earlier findings that the experimental and theoretical densities closely resemble each other in terms of their values, but can considerably differ in terms of their curvatures at the BCP. For both molecules, the experimental $\nabla^2\rho_{BCP}$ values are consistently less negative than the theoretical ones for all bonds except for the C—N bonds in the pyrrole rings and the C—F bond for **PP4F**.

The BCPs of all aromatic C—C bonds in the phenyl ring of **PP** are slightly shifted toward the C-atom located closer to the electronegative nitrogen atom. This is accompanied by an increase/decrease in the $\rho(\mathbf{r}_{BCP})/\nabla^2\rho(\mathbf{r}_{BCP})$ values for all but the C1—C2 and C1—C6 bonds. No quinoidal character for the phenyl ring can be deduced from the bond topological indices.

The comparison of the Laplacian along the N—C bond paths of **PP** and both molecules of **PP4F** shows that these bonds are almost identical in terms of the spatial arrangement of charge concentrations (Figure 6). The same graphs for the different bonds show an increased polarity in the sequence C—C, N—C, and F—C, as can be seen by an increased bonded valence shell charge concentration near the more electronegative atom.

The AIM charge of the nitrogen atom in **PP** is more negative than that in **PP4F** (see Table 5). The polarization introduced by the N-atom is mirrored in the charges of the carbon atoms in **PP**. The C-atom bonded to the N-atom (C11) has a distinct positive charge, while the other carbon atoms in the phenyl ring are increasingly negative with increasing distance to the nitrogen atom. In **PP4F**, the carbon atoms of the phenyl ring at the 2-, 3-, 5-, and 6-positions (C2/C12 and C3/C13) are almost neutral, while those bonded to the electronegative N- and F-atoms (C1 and C4) exhibit positive charges. The theoretically derived charges are systematically shifted to more positive values for all atoms in the pyrrole ring and the carbon atoms in 2-, 3-, 4-, 5-, and 6-positions in the phenyl ring. In contrast, C1 and all hydrogen atoms are more negative than those in the experiment. Individual comparison of theoretically and experimentally derived charges show occasionally distinct differences; however, there is an overall correlation with agreement greater than 73% (**PP**; a linear regression between the charges *Q* yields: $Q_{exp} = 1.1185Q_{theo} + 0.0003$; $R^2 = 0.7364$) and 94% (**PP4F**; $Q_{exp} =$

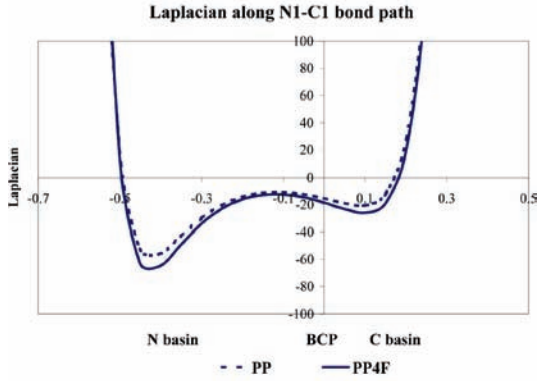

(a)

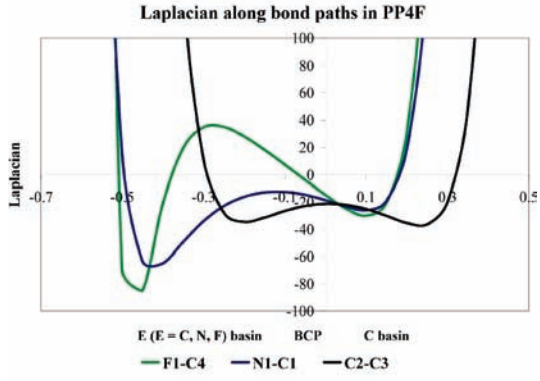

(b)

Figure 6. Laplacian along the bond paths in **PP** and **PP4F**. (a) Comparison of the N—C_{ipso} bonds in **PP** and **PP4F**. (b) Comparison of three bonds with different polarity in **PP4F**. The *x*-axis gives the distance to the BCP in Å and the *y*-axis the Laplacian in e Å^{-5}.

TABLE 5: Experimentally and Theoretically Derived Charges and Volumes from the Integration of the Electron Density over the Atomic Basins in PP and PP4F[a]

	PP		PP4F	
	charge[b] [e]	volume[b] [Å^3]	charge [e]	volume [Å^3]
N1/N11	−1.36	12.67	−1.20/−1.23	12.12/12.32
	−1.21	*11.63*	*−1.21*	*11.52*
C1/C11	+0.61	8.08	+0.39/+0.45	8.87/8.39
	+0.33	*9.20*	*+0.35*	*9.11*
C2/C12	−0.11	12.35	−0.04/−0.09	12.00/12.24
	−0.01	*11.98*	*0.00*	*11.75*
C3/C13	−0.31	12.89	−0.08/−0.12	12.23/12.25
	+0.02	*12.15*	*+0.03*	*11.82*
C4/C14	−0.34	13.08	+0.49/+0.36	9.09/9.49
	−0.01	*12.24*	*+0.51*	*8.91*
F1/F11			−0.61/−0.70	15.72/15.83
			−0.68	*16.11*

[a] The total molecular volumes are 188.48 Å^3/194.44 Å^3 for **PP** (exp/theor) and 192.44 Å^3/191.32 Å^3 for **PP4F** (exp/theor). [b] Values in italics are from theoretical calculations of **PP** and **PP4F**. Theoretical charges are calculated with DGrid[29] and volumes with AIM2000.[28]

$0.9377Q_{theo} + 0.0002$; $R^2 = 0.9407$). The larger variation in the case of **PP** may be attributed to the larger difference in the dihedral angle between the phenyl and the pyrrole ring from theory and experiment, which has an impact on the dipole moment and on atomic charges. A trend to reduced atomic volumes for carbon atoms bonded to more electronegative partners like N and F is observed.

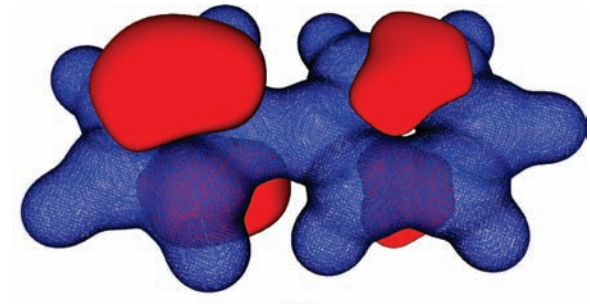

(a)

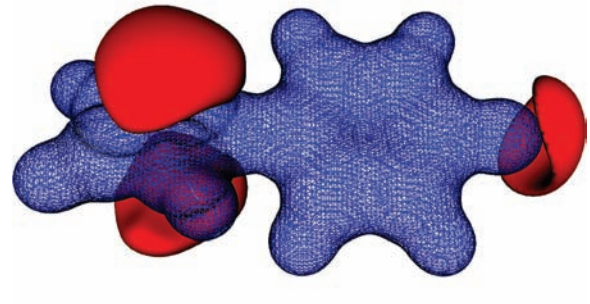

(b)

Figure 7. Electrostatic potential of **PP** (a) and **PP4F** (b) in the solid state. The red isosurfaces represent the negative potential at the −0.065 e Å^{-1} level and the blue isosurfaces the positive potential at the +0.300 e Å^{-1} level.

X-ray charge density is a unique technique to derive all three components of the dipole vector of molecules in the solid phase. For **PP**, the dipole vector is found to be oriented along the C—N bond vector (from C1 to N1) with a magnitude of 1.92 D, indicating a slight enhancement relative to that observed for the liquid state (1.39 D).[31]

The dipole moment in **PP4F** is oriented in the same direction (from C1 to N1, 3.01 D, and 3.28 D for the two independent molecules). In the liquid state a dipole moment of 0.32 D[1e] is observed; however, its direction cannot be determined reliably.

The results from gas-phase optimizations are −1.46 D (i.e., opposite direction compared to the experimental result) for **PP** and 0.01 D (i.e., in the same direction but considerably weaker than that in the experiment) for **PP4F**. Comparing the dipole moments from C_{2v} geometry restricted optimizations at the same level of theory (B3LYP/cc-pVTZ) with dihedral angles set to 90° (−0.60 D) and to 180° (+0.41 D) shows that the dipole moment is extremely sensitive to changes in the dihedral angle, which, in turn, is strongly affected by the crystal environment. Therefore, the comparison of such values should be taken with caution.

Figure 7 shows a comparison of the color-coded isosurface representations of the electrostatic potential for the molecules. This function, calculated from the solid state multipole ED and in principle including all crystal-field effects, reveals features that are less apparent in the density. While the negative potential is located mainly above and below the aromatic ring systems in **PP**, it is shifted from the phenyl ring to the F-atom in **PP4F**. The areas with negative potentials on the top and bottom of the pyrrole ring are polarized toward the nitrogen atom in both compounds. Since the potentials are almost identical in the two molecules of **PP4F**, only one is depicted in this plot.

Conclusion

The results of the multipole refinements and the topological analyses affirm that it is possible to extract a reliable electron density distribution even from a disordered structure, provided that the scattering power is high and proper constraints are imposed on the multipole refinement. A residual density analysis proves that no systematic errors in the residual density distribution, i.e., no features, remain in the entire unit cell after taking the disorder into account.

In conclusion, we regard the results discussed here to be important for recent research in chemistry, as they guide the way to charge density studies even for disordered structures. Many crystals contain coordinated or noncoordinated solvent molecules that suffer from disorder. Even those problematic crystal structures might be promising candidates for charge density studies in the future.

Acknowledgment. This work was supported by the Deutsche Forschungsgemeinschaft (Priority program 1178: Experimental electron density as the key to understand chemical bonding) and Chemetall, Frankfurt/Main. Author G.M.S. acknowledges support from the Fonds der Chemischen Industrie. The authors are thankful for the valuable comments from the referees.

Supporting Information Available: Detailed crystallographic information on independent atom model- and multipole model refinement as well as from theoretical calculations for **PP** and **PP4F**. This information is available free of charge via the Internet at http://pubs.acs.org. CCDC-231708 (**PP**) and CCDC-231707 (**PP4F**) contain the supplementary crystallographic data for this paper. This data can be obtained free of charge from The Cambridge Crystallographic Data Centre via www.ccdc.cam.ac.uk/data_request/cif.

References and Notes

(1) (a) Yoshihara, T.; Druzhinin, S. I.; Zachariasse, K. A. *J. Am. Chem. Soc.* **2004**, *126*, 8535. (b) Yoshihara, T.; Druzhinin, S. I.; Demeter, A.; Kocher, N.; Stalke, D.; Zachariasse, K. A. *J. Phys. Chem. A* **2005**, *109*, 1497. (c) Druzhinin, S. I.; Kovalenko, S. A.; Senyushkina, T. A.; Demeter, A.; Machinek, R.; Noltemeyer, M.; Zachariasse, K. A. *J. Phys. Chem. A* **2008**, *112*, 8238. (d) Druzhinin, S. I.; Kovalenko, S. A.; Senyushkina, T. A.; Demeter, A.; Machinek, R.; Noltemeyer, M.; Zachariasse, K. A. *J. Phys. Chem. A* **2009**, *113*, 520. (e) Druzhinin, S. I.; Kovalenko, S. A.; Senyushkina, T. A.; Demeter, A.; Januskevicius, R.; Mayer, P.; Stalke, D.; Machinek, R.; Zachariasse, K. A., *J. Phys. Chem. A*, **2009**, DOI: 10.1021/jp903613c.

(2) Grabowski, Z. R.; Rotkiewicz, K.; Rettig, W. *Chem. Rev.* **2003**, *103*, 3899.

(3) Heine, A.; Herbst-Irmer, R.; Stalke, D.; Kühnle, W.; Zachariasse, K. A. *Acta Crystallogr.* **1994**, *B50*, 363.

(4) Hansen, N. K.; Coppens, P. *Acta Crystallogr.* **1978**, *A34*, 909.

(5) Bürgi, H.-B.; Capelli, S. C. *Helv. Chim. Acta* **2003**, *86*, 1625.

(6) (a) Kim, C. D.; Pillet, S.; Wu, G.; Fullagar, W. K.; Coppens, P. *Acta Crystallogr.* **2002**, *A58*, 133. (b) Coppens, P.; Ma, B.; Gerlits, O.; Zhang, Y.; Kulshrestha, P. *CrystEngComm* **2002**, *4*, 302. (c) Coppens, P.; Novozhilova, I. V. *Faraday Discuss.* **2003**, *122*, 1.

(7) (a) Yufit, D. S.; Howard, J. A. K.; Davidson, M. G. *J. Chem. Soc., Perkin Trans.* **2000**, *2*, 249. (b) Tafipolsky, M.; Scherer, W.; Öfele, K.; Artus, G.; Pedersen, B.; Herrmann, W. A.; McGrady, G. S. *J. Am. Chem. Soc.* **2002**, *124*, 5865. (c) Messerschmidt, M.; Wagner, A.; Wong, M. W.; Luger, P. *J. Am. Chem. Soc.* **2002**, *124*, 732. (d) Leusser, D.; Henn, J.; Kocher, N.; Engels, B.; Stalke, D. *J. Am. Chem. Soc.* **2004**, *126*, 1781. (e) Kocher, N.; Henn, J.; Gostevskii, B.; Kost, D.; Kalikhman, I.; Engels, B.; Stalke, D. *J. Am. Chem. Soc.* **2004**, *126*, 5563. (f) Spackman, M. A. *Annu. Rep. Prog. Chem., Sect. C: Phys. Chem.* **1998**, *94*, 177. (g) Koritsanszky, T. S.; Coppens, P. *Chem. Rev.* **2001**, *101*, 1583. (h) Ott, H.; Däschlein, C.; Leusser, D.; Schildbach, D.; Seibel, T.; Stalke, D.; Strohmann, C. *J. Am. Chem. Soc.* **2008**, *130*, 11901. (i) Flierler, U.; Burzler, M.; Leusser, D.; Henn, J.; Ott, H.; Braunschweig, H.; Stalke, D. *Angew. Chem.* **2008**, *120*, 4393. Flierler, U.; Burzler, M.; Leusser, D.; Henn, J.; Ott, H.; Braunschweig, H.; Stalke, D. *Angew. Chem., Int. Ed.* **2008**, *47*, 4321.

(8) (a) Jelsch, C.; Pichon-Pesme, V.; Lecomte, C.; Aubry, A. *Acta Crystallogr.* **1998**, *D54*, 1306. (b) Housset, D.; Benabicha, F.; Pichon-Pesme, V.; Jelsch, C.; Maierhofer, A.; David, S.; Fontecilla-Camps, J. C.; Lecomte, C. *Acta Crystallogr.* **2000**, *D56*, 151. (c) Jelsch, C.; Teeter, M. M.; Lamzin, V.; Pichon-Pesme, V.; Blessing, R. H.; Lecomte, C. *Proc. Natl. Acad. Sci. U.S.A.* **2000**, *97*, 3171. (d) Lecomte, C.; Guillot, B.; Muzet, N.; Pichon-Pesme, V.; Jelsch, C. *Cell. Mol. Life Sci.* **2004**, *61*, 774. (e) Dittrich, B.; Koritsanszky, T.; Volkov, A.; Mebs, S.; Luger, P. *Angew. Chem.* **2007**, *119*, 2993. Dittrich, B.; Koritsanszky, T.; Volkov, A.; Mebs, S.; Luger, P. *Angew. Chem., Int. Ed.* **2007**, *46*, 2935.

(9) Meindl, K.; Henn, J. *Acta Crystallogr.* **2008**, *A64*, 404.

(10) *SMART-NT: Program for Diffractometer Controlling*; Bruker AXS Inc.: Madison, WI, 2000.

(11) (a) Kottke, T.; Stalke, D. *J. Appl. Crystallogr.* **1993**, *26*, 615. (b) Kottke, T.; Lagow, R. J.; Stalke, D. *J. Appl. Crystallogr.* **1996**, *29*, 465. (c) Stalke, D. *Chem. Soc. Rev.* **1998**, *27*, 171.

(12) *SAINT-NT: Program for Integration of Diffraction Data from Area Detectors*; Bruker AXS Inc.: Madison, WI, 2000.

(13) Sheldrick, G. M. *SADABS 2.05: Program for Area Detector Absorption Correction*; University of Göttingen; Göttingen, Germany, 2002.

(14) *SHELXTL-97*; Bruker AXS Inc.: Madison, WI, 1997.

(15) Sheldrick, G. M. *Acta Crystallogr.* **1990**, *A46*, 467.

(16) Sheldrick, G. M. *Acta Crystallogr.* **2008**, *A64*, 112.

(17) Sheldrick, G. M.; Schneider, T. R. *Methods Enzymol.* **1997**, *277*, 319.

(18) Volkov, A.; Abramov, Y.; Coppens, P.; Gatti, C. *Acta Crystallogr.* **2000**, *A56*, 332.

(19) Allen, F. *Acta Crystallogr.* **1986**, *B42*, 515.

(20) Volkov, A.; Macchi, P.; Farrugia, L. J.; Gatti, C.; Mallinson, P. R.; Richter, T.; Koritsanszky, T. *XD2006 — A Computer Program Package for Multipole Refinement, Topological Analysis of Charge Densities and Evaluation of Intermolecular Energies from Experimental and Theoretical Structure Factors*, State University of New York: Buffalo, 2006.

(21) Clementi, E.; Raimondi, D. L. *J. Chem. Phys.* **1963**, *38*, 2686.

(22) Volkov, A.; Abramov, Y. A.; Coppens, P. *Acta Crystallogr.* **2001**, *A57*, 272.

(23) Hirshfeld, F. L. *Acta Crystallogr.* **1976**, *A32*, 239.

(24) Frisch, M. J.; Trucks, G. W.; Schlegel, H. B.; Scuseria, G. E.; Robb, M. A.; Cheeseman, J. R.; Montgomery, J. A., Jr.; Vreven, T.; Kudin, K. N.; Burant, J. C.; Millam, J. M.; Iyengar, S. S.; Tomasi, J.; Barone, V.; Mennucci, B.; Cossi, M.; Scalmani, G.; Rega, N.; Petersson, G. A.; Nakatsuji, H.; Hada, M.; Ehara, M.; Toyota, K.; Fukuda, R.; Hasegawa, J.; Ishida, M.; Nakajima, T.; Honda, Y.; Kitao, O.; Nakai, H.; Klene, M.; Li, X.; Knox, J. E.; Hratchian, H. P.; Cross, J. B.; Bakken, V.; Adamo, C.; Jaramillo, J.; Gomperts, R.; Stratmann, R. E.; Yazyev, O.; Austin, A. J.; Cammi, R.; Pomelli, C.; Ochterski, J. W.; Ayala, P. Y.; Morokuma, K.; Voth, G. A.; Salvador, P.; Dannenberg, J. J.; Zakrzewski, V. G.; Dapprich, S.; Daniels, A. D.; Strain, M. C.; Farkas, O.; Malick, D. K.; Rabuck, A. D.; Raghavachari, K.; Foresman, J. B.; Ortiz, J. V.; Cui, Q.; Baboul, A. G.; Clifford, S.; Cioslowski, J.; Stefanov, B. B.; Liu, G.; Liashenko, A.; Piskorz, P.; Komaromi, I.; Martin, R. L.; Fox, D. J.; Keith, T.; Al-Laham, M. A.; Peng, C. Y.; Nanayakkara, A.; Challacombe, M.; Gill, P. M. W.; Johnson, B.; Chen, W.; Wong, M. W.; Gonzalez, C.; Pople, J. A. *Gaussian 03, Revision D.01*; Gaussian, Inc.: Wallingford, CT, 2003.

(25) (a) Rückert, I.; Hebecker, A.; Parusel, A. B. J.; Zachariasse, K. A. *Z. Phys. Chem.* **2000**, *214*, 1597. (b) Demeter, A.; Druzhinin, S.; George, M.; Haselbach, E.; Roulin, J.-L.; Zachariasse, K. A. *Chem. Phys. Lett.* **2000**, *323*, 351.

(26) Rademacher, P. *Strukturen organischer Moleküle*; VCH: Weinheim, Germany, 1987.

(27) (a) Desiraju, G. R.; Steiner, T. *The Weak Hydrogen Bond In Structural Chemistry and Biology*; Oxford University Press: Oxford, 1999. (b) Steiner, T. *Angew. Chem.* **2002**, *114*, 50. Steiner, T. *Angew. Chem., Int. Ed.* **2002**, *41*, 48.

(28) Biegler-König, F.; Schönbohm, J.; Bayles, D. *J. Comput. Chem.* **2001**, *22*, 545.

(29) Kohout, M. *DGrid, v 4.4*; Radebeul, 2008.

(30) Bader, R. F. W. *Atoms in Molecules: A Quantum Theory*; Oxford University Press: Oxford, 1990.

(31) Lumbroso, H.; Bertin, D. M.; Marschner, F. *J. Mol. Struct.* **1988**, *178*, 187.

JP9026157